Ultrasound in Med. & Biol., Vol. 46, No. 7, pp. 1715–1726, 2020

0301-5629/$ - see front matter

https://doi.org/10.1016/j.ultrasmedbio.2020.03.005

● *Original Contribution*

IN VIVO ULTRAFAST QUANTITATIVE ULTRASOUND AND SHEAR WAVE ELASTOGRAPHY IMAGING ON FARM-RAISED DUCK LIVERS DURING FORCE FEEDING

Marc Gesnik,* Manish Bhatt,* Marie-Hélène Roy Cardinal,* François Destrempes,* Louise Allard,* Bich N. Nguyen,† Thierry Alquier,‡,§ Jean-François Giroux,¶ An Tang,‖,#,**,†† and Guy Cloutier*,#,††

* Laboratory of Biorheology and Medical Ultrasonics, University of Montreal Hospital Research Center (CRCHUM), Montréal, QC, Canada; † Service of Pathology, University of Montreal Hospital (CHUM), Montréal, QC, Canada; ‡ CRCHUM and Montreal Diabetes Research Center, Montréal, QC, Canada; § Department of Medicine, University of Montreal, Montréal, QC, Canada; ¶ Department of Biological Sciences, University of Quebec in Montreal, Montréal, QC, Canada; ‖ Service of Radiology, University of Montreal Hospital (CHUM), Montréal, QC, Canada; # Department of Radiology, Radio-Oncology and Nuclear Medicine, University of Montreal, Montréal, QC, Canada; ** Laboratory of Medical Image Analysis, University of Montreal Hospital Research Center (CRCHUM), Montréal, QC, Canada; and †† Institute of Biomedical Engineering, University of Montreal, Montréal, QC, Canada

(*Received* 22 *October* 2019; *revised* 5 *February* 2020; *in final from* 10 *March* 2020)

Abstract—Shear wave elastography (speed and dispersion), local attenuation coefficient slope and homodyned-*K* parametric imaging were used for liver steatosis grading. These ultrasound biomarkers rely on physical interactions between shear and compression waves with tissues at both macroscopic and microscopic scales. These techniques were applied in a context not yet studied with ultrasound imaging, that is, monitoring steatosis of force-fed duck livers from pre-force-fed to *foie gras* stages. Each estimated feature presented a statistically significant trend along the feeding process (p values $<10^{-3}$). However, whereas a monotonic increase in the shear wave speed was observed along the process, most quantitative ultrasound features exhibited an absolute maximum value halfway through the process. As the liver fat fraction in *foie gras* is much higher than that seen clinically, we hypothesized that a change in the ultrasound scattering regime is encountered for high-fat fractions, and consequently, care has to be taken when applying ultrasound biomarkers to grading of severe states of steatosis. (E-mail: guy.cloutier@umontreal.ca)

Key Words: **Shear wave elastography, Shear wave dispersion, Quantitative ultrasound, Homodyned *K*-distribution, Local attenuation, Liver steatosis, Duck *foie gras*, Histopathology.**

INTRODUCTION

Non-alcoholic fatty liver disease (NAFLD), including non-alcoholic steatohepatitis (NASH), is an ever-growing condition that often evolves to advanced stages (cirrhosis and cancer) in humans (Vernon et al. 2011). Current reference methods for NAFLD grading are tissue sampling by biopsy (Kleiner et al. 2005; Sanyal et al. 2011), computed tomography (CT) (Ricci et al. 1997) and magnetic resonance-based techniques (Bonekamp et al. 2014; Yokoo et al. 2018; Qu et al. 2019) that are able to grade steatosis through direct estimation of the liver fat fraction. However, because of the large number of potentially affected patients, screening for early stages of NAFLD cannot be done using these techniques, biopsy being too invasive, CT being associated with ionizing radiation and magnetic resonance imaging being too costly and lacking availability.

On the other hand, ultrasound is a promising and cost-effective imaging method for early steatosis grading (Loomba 2018; Ozturk et al. 2018; Zhang et al. 2018; Castera et al. 2019; Tada et al. 2019a). Ultrasound methods indirectly estimate ultrasound physics-based biomarkers, such as tissue viscoelasticity (Barry et al. 2012,

Address correspondence to: Guy Cloutier, Laboratory of Biorheology and Medical Ultrasonics, Centre de Recherche du Centre Hospitalier de l'Université de Montréal (CRCHUM), 900 St-Denis, Suite R11.720, Montréal, Québec H2X 0A9, Canada. E-mail: guy.cloutier@umontreal.ca

2014, 2015; Deffieux et al. 2015; Nightingale et al. 2015; Parker et al. 2018; Sharma et al. 2019), ultrasound attenuation (Nam et al. 2011; De Lédinghen et al. 2014; Sasso et al. 2016; Karlas et al. 2017; Tada et al. 2019a, 2019b), speed of sound (Imbault et al. 2017; Dioguardi Burgio et al. 2019), spectral backscattering properties (Lin et al. 2015, 2018; Lee et al. 2017) and scatterer acoustical properties and spatial organization through echo-envelope statistics (Ghoshal et al. 2012; Fang et al. 2018; Zhou et al. 2019). Even though these physical features describing ultrasound compression or shear wave propagation are plausibly linked to liver cellular changes and fat fraction increase during steatosis, this link remains unclear. Some other recent efforts toward characterization of mechanical properties of different tissues include computation of group shear wave speed (SWS) (displacement, velocity and acceleration group speed) on tissue-mimicking phantoms (Rouze et al. 2018) and assessment of the viscoelastic response in human muscles (Moore et al. 2018).

To improve the classification of liver steatosis, multiparametric ultrasound imaging modalities have been investigated. When applied to fatty liver animal models, multiparametric methods exhibited increased performance in steatosis, NASH and fibrosis classifications by combining shear wave elastography with spectral-based features (Franceschini et al. 2019) or, additionally, echo-envelope features (Tang et al. 2019). However, these animal models were assessed under experimental diets, such as methionine- and choline-deficient feeding, to mimic human NASH. With these animal models, the encountered steatosis fat fraction can reach 30%−40% for severe cases, but the fatty liver is mixed with inflammation and fibrosis (Weltman et al. 1996; Bonnefont et al. 2019).

For a better understanding of the link between ultrasound biomarkers and steatotic parenchyma only, ultrasound imaging of the Mulard duck's liver during force-feeding was investigated. The ability of Mulard ducks (*Anas platyrhynchos domesticus* × *Cairina moschata*) to reversibly develop extreme steatosis under controlled force-feeding has been extensively studied in poultry sciences for *foie gras* production (Hermier et al. 1999; Locsmándi et al. 2007; Baéza et al. 2013; Bonnefont et al. 2019). Within 2 wk of feeding, the volumetric liver fat fraction can increase from negligible to more than 60% in these animals.

Leveraging this reproducible severe state of liver steatosis and the portability of ultrasound scanners, this study aimed to design an *in vivo* duck liver multiparametric ultrasound imaging protocol, during force-feeding, that could be directly conducted at the farm for liver steatosis monitoring. Four state-of-the-art ultrasound tools were used at four time points during the feeding process to investigate non-invasively various fatty liver states, from pre-force-fed to *foie gras*. Tested imaging technologies were SWS estimation, SWS dispersion, local attenuation coefficient slope (ACS) estimation and homodyned-*K* distribution (HKD) parametric images.

METHODS

Animal procedure

This study received approval from the Institutional Animal Care Committee of the University of Montreal Hospital Research Center. Sixteen Mulard ducks were included in this study. They were housed collectively in a barn with free access to water. The feeding process consisted of 14 d of pre-force-feeding (ranging from day −13 to day 0), followed by 14 d of force-feeding (ranging from day 1 to day 14). During the pre-force-feeding period, access to food was limited in time, so that ducks became accustomed to ingurgitating a great quantity of food over a short period. During the force-feeding period, ducks were fed twice a day with an increasing amount of re-humidified full corn grains for 10−20 s each time (approximately 350 g per feeding at the beginning and 650 g at the end, composed of 40% water and 60% dried corn grains).

Ducks underwent liver ultrasound imaging sessions at four time points during the pre-feeding and force-feeding periods (days −12, 0, 7 and 14). Animals were handled by a veterinarian during imaging, which was conducted directly in the housing farmhouse. While the animal was awake (no anesthesia) and manually held on its back, an approximately 8 × 8-cm^2 patch of skin over the liver's position was plucked and cleaned with water and alcohol before applying acoustic coupling gel for ultrasound imaging. For each duck, an imaging session lasted about 10 min. After completion of the feeding process, animals were sent to a slaughterhouse, where they were sacrificed for commercial production of *foie gras* (fatty duck liver).

Two liver samples from the right and left lobes of a randomly selected specimen (duck 15) were kept for histopathology analysis at day 14. The liver sample was fixed in a 10% formalin solution within 4 min of animal euthanasia. The liver specimen was subsequently stained with hematoxylin and eosin and Masson's trichrome. Histology slides were assessed by a liver pathologist according to the NASH Clinical Research Network scoring system (Kleiner et al. 2005). The assessment included steatosis grade (0−3), lobular inflammation (0−3), hepatocellular ballooning (0−2) and fibrosis (0−4).

Ultrasound data acquisition

Ultrasound scanning was performed with a Verasonics V1 programmable system (Verasonics, Kirkland, WA, USA) using an ATL L7-4 linear probe (Philips,

Bothell, WA, USA) driven at 5 MHz. Once the probe was positioned above the liver based on real-time B-mode imaging, the localization of acoustic pushes was manually selected beyond the skin and fat layers at a depth of at most 1 cm within the liver, and the scanner was then switched to the acquisition mode. An acquisition lasted 61 ms and consisted of 100 plane wave frames at the rate of 3086 Hz for quantitative ultrasound (QUS) assessment, followed immediately by three acoustic pushes lasting 198.4 μs each and separated by 2.5 mm in depth, for shear wave elastography imaging (SWEI) and 100 frames at the rate of 3623 Hz for shear wave tracking. The acoustic radiation pressure push was made with 64 elements of the transducer.

After data acquisition, a quick suboptimal image reconstruction was performed for visual display. Each reconstructed frame was the compounded coherent sum of three angulated plane waves at -1°, 0° and 1°, resulting in pulse repetition frequencies of 9259 Hz for plane wave QUS and 10,870 Hz for shear wave displacement tracking. The visual quality assessment during experiments was based on in-phase and quadrature signal beamforming using Verasonics software. The propagating shear waves were displayed, and the contour of the liver was manually delineated. Raw radiofrequency (RF) data were saved for subsequent optimized beamforming and data post-processing.

Two to four acquisitions were performed per duck. Alongside acquisitions, reference acquisitions for QUS were conducted on a reference phantom (117 GU-101, CIRS, Norfolk, VA, USA). The attenuation coefficient α_{ref} and backscatter coefficient BSC_{ref} were provided by the manufacturer: $\alpha_{\text{ref}} = 0.72$ dB/cm/MHz, and BSC_{ref} (at 3 MHz) $= 1.24 \times 10^{-3}$/str/cm). The final beamforming was performed afterward using the f–k migration method (Garcia et al. 2013). Offline post-processing was done using MATLAB software (The MathWorks Inc., Natick, MA, USA).

Shear wave speed and dispersion estimation

For each RF acquisition, the velocity field $v_z(x, z, t)$ was computed using 2-D auto-correlations (Loupas et al. 1995). The liver parenchyma was assumed to be locally homogeneous, and its stiffness was estimated using the shear wave phase velocity (Deffieux et al. 2009). The estimation was performed over a 1×1-cm square region-of-interest (ROI) enclosed within the liver identified on B-mode images. The ROI was selected in the liver region where relatively lesser noisy wave fields were observed. The velocity field was then averaged over depth z within the ROI. This step yielded a 2-D mean velocity field $\overline{v_z}(x,t)$ describing the shear wave propagation inside the assumed homogeneous and purely elastic ROI (Chen et al. 2004).

The phase velocity, c_φ, at 400 Hz was estimated using a linear fitting of the phase function along the lateral position x (Deffieux et al. 2009). The 400-Hz frequency corresponds to the upper shear wave frequency bandwidth and was selected based on observations made by Kazemirad et al. (2017). For each shear wave acquisition, the goodness-of-fit of the phase velocity linear function was assessed with the coefficient of determination (R^2) defined as

$$R^2 = 1 - \frac{\sum_i ||y_i - \hat{y}_i||^2}{\sum_i ||y_i - \overline{y}||^2} \quad (1)$$

where $y = [y_1, y_2, \ldots, y_n]$ is the data set of phase values, and $\overline{y}$ is its mean value, whereas $\hat{y} = [\hat{y}_1, \hat{y}_2, \ldots, \hat{y}_n]$ is the corresponding predicted values under the linear fit. The estimated shear wave velocity was rejected whenever $R^2 < 0.9$ (Bouchard et al. 2009; Yu et al. 2009), which can be interpreted as meaning that less than 90% of the total variance is explained by the estimated linear model. Estimated shear wave speeds meeting that criterion were averaged to a single value per duck per imaging session between days −12 to 14.

Barry et al. (2012, 2014, 2015) reported that dispersion of the SWS can be correlated with the degree of liver steatosis. The SWS dispersion can be estimated as the slope of the shear wave phase velocity versus shear wave frequency (Barry et al. 2012). Here, the phase velocity was computed over the accessible bandwidth (75–400 Hz) and plotted against frequency; and the slope of the linear fit yielded the dispersion.

Local ACS estimation

The local ACS was estimated with the spectral log difference (SLD) method using measures proximal and distal to the ROI (Insana et al. 1983; Labyed and Bigelow 2011; Coila and Lavarello 2018). The SLD method was chosen because of its small estimation variance (Labyed and Bigelow 2011) and the assumption of some variation in scattering properties over the selected ROI. The ROI size was chosen as 20 scan lines in the lateral direction and 40 pulse lengths in the axial direction. SLD proximal and distal window lengths were 20 pulse lengths long. Window overlaps of 75% and 87.5% were used in the lateral and axial directions, respectively, to compute ACS. After discrete Fourier transforms were performed, power spectra were averaged along scan lines. The usable frequency range was chosen as the −20-dB bandwidth boundaries with respect to the peak power spectrum. For each acquisition, ACS maps were averaged over the 100 frames of the ROI liver region and then averaged again over available number of acquisitions (2–4) to yield a single ACS value per duck per imaging session.

Homodyned-K *feature estimation*

The statistical property of the RF echo envelope was modeled with the HKD (Dutt and Greenleaf 1994; Destrempes and Cloutier 2010). To reduce acquisition noise, the average over each non-overlapping set of 10 consecutive compounded RF frames within an acquisition was computed, resulting in sequences of 10 frames. Echo envelope images were computed by applying the Hilbert transform on averaged RF frames. HKD parameters were estimated on sliding windows of 8 pulse lengths × 17 scan lines, corresponding to approximately 5 mm in both the axial and lateral directions, which were swept across the liver ROI by steps of 0.5 pulse length × 1 scan line (Destrempes and Cloutier 2013; Destrempes et al. 2016). In particular, pixels within the ROI were classified into three or fewer labels according to their statistical echogenic properties (Destrempes et al. 2016), so that the hypothesis of a single homodyned K-distribution was met for each estimation by considering only pixels within the sliding window at a given position that had the same label as the window's current geometric center, as described in Destrempes and Cloutier (2013).

The HKD parameters included mean intensity μ_n (square of the echo-envelope amplitude), the reciprocal $1/\alpha$ of the scatterer clustering parameter, related to the density of scatterers and homogeneity of fluctuations in acoustical impedance, and the coherent-to-diffuse signal ratio k, related to the presence of structure in the spatial organization of scatterers or the presence of specular reflection. Each of the three HKD parameters was averaged over the ROI liver region, and the median over the 10 echo envelope frames were output. For each HKD parameter, the average value over the available number of acquisitions (2−4) yielded a single value per duck per imaging session.

Statistical analysis

Descriptive statistics are reported as means ± 1 standard deviation (SD). As there are multiple feeding time points, the Kruskal−Wallis one-way analysis of variance was used to test if one feeding time differed from the others. For each ultrasound feature, in case of a statistically significant Kruskal−Wallis one-way analysis with confidence level $\alpha < 0.05$, multiple comparisons of the feature were performed at all feeding time pairs using Mann−Whitney tests. The Holm−Bonferroni method was applied to adjust p values of multiple comparisons. Statistical analyses were performed with *R* software (Version 3.2.5; The *R* Foundation for Statistical Computing, Vienna, Austria, https://www.r-project.org).

RESULTS

Figure 1a is a B-mode image of an *in vivo* duck liver. Figure 1 (b−d) illustrate the segmented liver region, propagating shear wave field and phase-versus-distance linear fit for SWS estimation. In Figure 2, individual ultrasound features along the feeding process are illustrated. Table 1 summarizes those values as well as

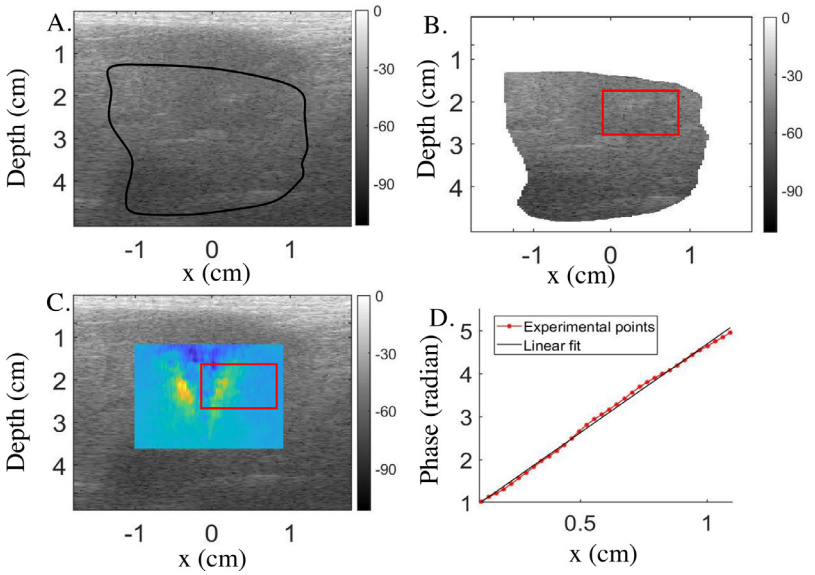

Fig. 1. Computation of the shear wave speed in an *in vivo* duck liver. (a) B-Mode image of the liver and surrounding tissues. The black contour outlines the liver. (b) Segmented liver region. The red rectangular box represents the region of interest within which shear wave speed computation was performed. (c) Representation of the shear wave field in the tissue. (d) Linear fitting of the phase function along the lateral distance x, the slope of which estimates the shear wave speed.

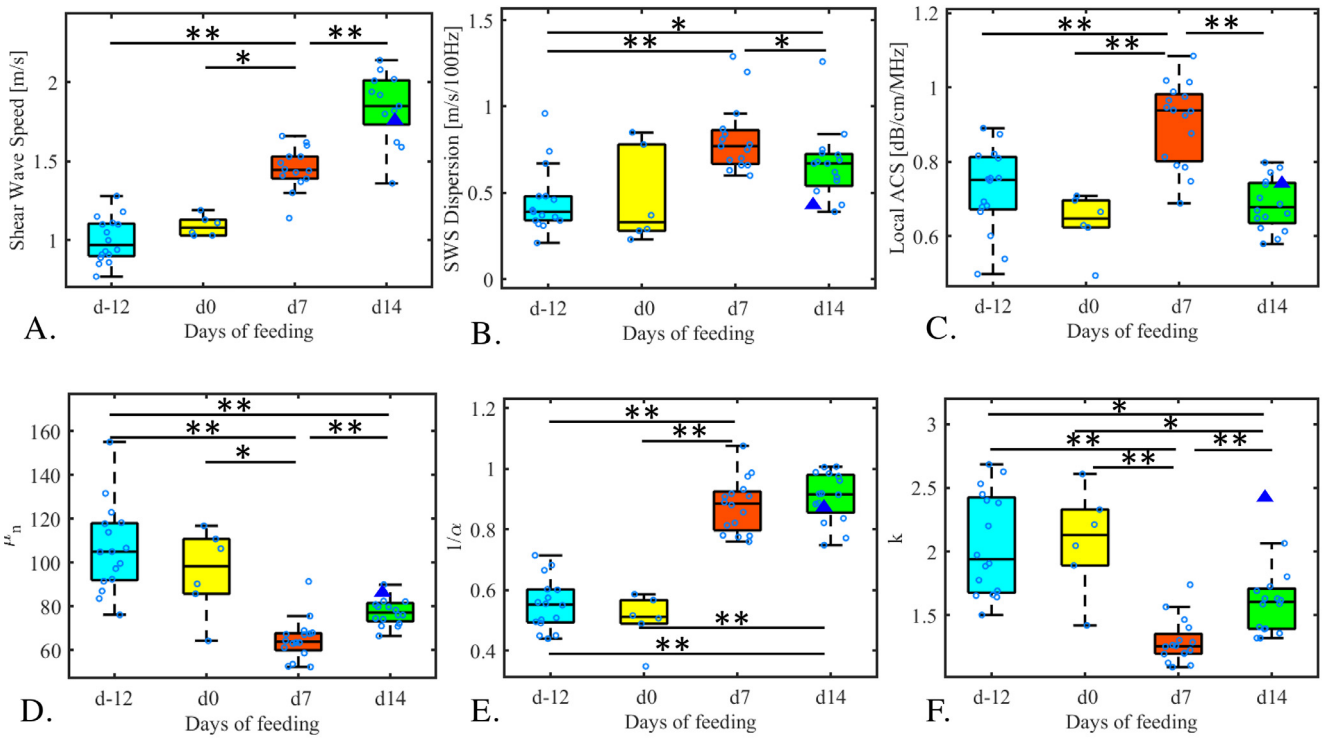

Fig. 2. Evolution of the measured ultrasound features in duck livers throughout the force-feeding process. Boxplots and scatterplots at days −12, 0, 7 and 14. At day 14, the sample identified with a triangle on each plot corresponds to the liver that went to histopathology (duck 15). (a) Shear wave speed. (b) Shear wave speed frequency dispersion. (c) Local attenuation coefficient slope (ACS). (d) Mean intensity μ_n of the homodyned K-distribution (HKD). (e) Reciprocal of the scatterer clustering parameter $1/\alpha$ of the HKD. (f) Coherent-to-diffuse signal ratio k of the HKD *p < 0.05, **p < 10^{-3}, Wilcoxon rank sum test.

Table 1. Ultrasound data collected at the four feeding time points*

	Day 12 (n = 16)†	Day 0 (n = 6)	Day 7 (n = 16)	Day 14 (n = 16)	p value (Kruskal−Wallis)
SWS (m/s)	1.00 ± 0.14	1.09 ± 0.06	1.45 ± 0.14	1.84 ± 0.22	4.9×10^{-9}
Fraction of SWEI acquisitions meeting R^2 criterion					
$R^2 \geq 0.9$	43/43 = 100%	17/17 = 100%	30/50 = 60%	23/45 = 51%	-
$R^2 \geq 0.95$	43/43 = 100%	17/17 = 100%	18/50 = 36%	7/45 = 16%	-
SWS dispersion (m/s/100 Hz)	0.40 ± 0.34	0.41 ± 0.27	0.81 ± 0.29	0.64 ± 0.23	9.9×10^{-8}
ACS (dB/cm/MHz)	0.72 ± 0.11	0.64 ± 0.08	0.91 ± 0.11	0.69 ± 0.07	7.1×10^{-6}
μ_n	106 ± 20	95.7 ± 20	64.8 ± 9.5	77.5 ± 6.2	5.6×10^{-8}
$1/\alpha$	0.69 ± 0.10	0.66 ± 0.15	0.90 ± 0.08	0.94 ± 0.07	5.2×10^{-8}
K	2.04 ± 0.39	2.06 ± 0.40	1.29 ± 0.17	1.61 ± 0.29	3.4×10^{-7}

ACS = attenuation coefficient slope; SWEI = shear wave elastography imaging; SWS = shear wave speed.

* The features are presented as averaged values over ducks per session ± one standard deviation. Only six ducks could be imaged at day 0 because of a critical ultrasound scanner failure. The fraction of SWEI acquisitions meeting the R^2 criterion is defined as the number of acquisitions meeting the criterion over the total number of acquisitions in the session. Total number of acquisitions per session varies because the number of acquisitions per duck varied between 2 and 4.

† n = number of imaged ducks.

the percentage of SWEI acquisitions per session that met the $R^2 \geq 0.9$ criterion (or $R^2 \geq 0.95$ criterion, for sake of comparison). As expected, no changes were observed during the pre-force-feeding period (day −12 vs. day 0) for all parameters. In contrast, all features individually exhibited a significant trend from pre-feeding to force-feeding periods (day 0 to day 14) ($p < 10^{-3}$, Kruskal−Wallis rank-sum test). SWS increased, indicating liver stiffening over time. SWS dispersion increased between days 0 and 7, but slightly decreased at day 14, as reported in Table 1. ACS increased between days 0 and 7, but decreased at day 14. The mean intensity μ_n

and coherent-to-diffuse signal ratio k exhibited similar but inverse behavior, reaching their minimum values at day 7, while the reciprocal $1/\alpha$ of the scatterer clustering parameter reached a plateau at day 7 (*i.e.*, no significant changes between days 7 and 14).

QUS features could be extracted at any time point with comparable variability (see Table 1, coefficients of variation varying between 7.4% and 22.3% for ACS, μ_n, $1/\alpha$ and k). On the other hand, the percentage of SWEI acquisitions per session meeting the $R^2 \geq 0.9$ criterion decreased along the process. The coefficients of variation at the four time points for the SWS data presented here were 14.0%, 5.5%, 9.6% and 12.0%, respectively. Larger values were obtained for the SWS dispersion (85.0%, 65.8%, 35.8% and 35.9%).

In Figure 3 are images of histology sections for duck 15. The pathology diagnosis of both left and right lobe specimens was panlobular steatosis grade 3 (>95% of hepatocytes containing fat), inflammation grade 3, hepatocellular ballooning grade 2, fibrosis grade 0.

DISCUSSION

A QUS and shear wave elastography liver imaging protocol was carried out *in vivo* on a cohort of 16 awake Mulard ducks throughout a force-feeding process. Liver steatosis in wild ducks is a natural and reversible process used to store energy for migration. In this study, force-fed animals were used as a model. From "healthy" to heavily steatotic livers, the effect of the controlled liver fat intake on state-of-the-art ultrasound biomarkers was investigated. Six features were studied, and statistically significant changes (with p values $<10^{-3}$) were observed over time during force-feeding. As steatosis is a diffuse liver disease in humans, it had been hypothesized that estimated biomarkers could be averaged over the segmented liver without loss of relevance. This was motivated by the variance of QUS estimators requiring spatial averaging to improve robustness. Because low-variance estimators were recently developed (Coila and Lavarello 2018; Vajihi et al. 2018), future studies may allow mapping of the spatial heterogeneity of duck fatty livers or human non-diffuse liver diseases.

Shear wave speed and dispersion estimation

Shear wave elastography results revealed that SWS increased almost twice from the beginning to the end of the force-feeding process, suggesting that the stiffness of duck *foie gras* is distinguishably higher than that of pre-force-fed livers. These patterns agree with previous studies performed on *ex vivo* liver samples (Tabaru et al. 2010; Bhatt et al. 2019). However, the proportion of the data set that could be used for SWS analysis was reduced to 60% at day 7 and 51% at day 14. This is most probably owing to pushing beam defocusing and energy loss caused by fat accumulation, as the pushing beam loses its kinetic energy as its travels within fatty tissues (Szabo 2004). This may also be owing to shear wave attenuation and frequency dispersion and to the fact that the signal-to-noise ratio (SNR) decreased with distance from the pushing beam because of viscous loss and extension of the shear wave tail (Parker et al. 2018). Ultimately, because attenuation increases with frequency, the phase velocity could only be estimated within a few millimeters of propagation, as also observed in Deffieux et al. (2009). Even though SWS featured a monotonic trend that could provide an interesting classification performance of its own, it cannot be reliably used exclusively because of this greater amount of unreliable data along the feeding process.

On the other hand, SWS dispersion results revealed an increase from day 0 to day 7, but a decrease at day 14. Barry et al. (2012) hypothesized in their human study that increasing the liver fat content would increase the slope of the dispersion measurement. The observed discrepancy might be attributed to the fat content, which is often less than 30% in humans, whereas the fat percentage in ducks can reach almost 60% at the end of the feeding process (Bonnefont et al. 2019).

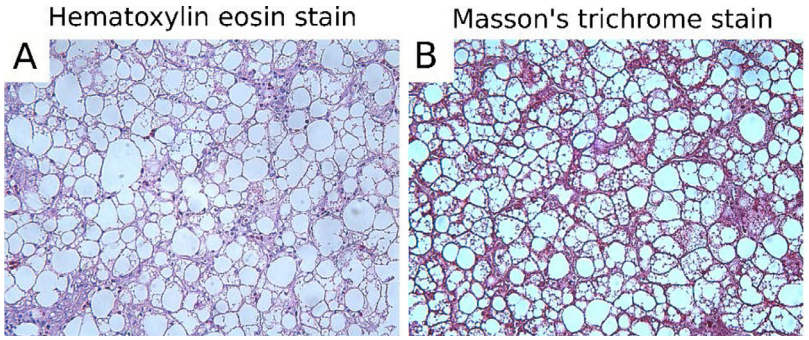

Fig. 3. Histopathology slides (magnification × 20) of the duck liver specimen at day 14. (a) Hematoxylin and eosin staining. (b) Masson's trichrome staining. The pathology diagnosis was the same for both left and right lobe specimens: panlobular steatosis grade 3 (>95%), inflammation grade 3, hepatocellular ballooning grade 2, fibrosis grade 0.

Alternative implementations of SWEI have been investigated to overcome the decrease in SNR caused by layers of fat. Future studies could consider harmonic imaging (Amador et al. 2016; Correia et al. 2016) because of its greater robustness to intervening aberrating layers. Passive elastography (Gallot et al. 2011) could also be of interest as breathing and heart motions propagate to the liver. Furthermore, obtaining better SNRs may allow for viscosity estimation, which was reported to be a feature of interest in steatosis grading (Deffieux et al. 2015; Nightingale et al. 2015; Bernard et al. 2017).

Local ACS estimation

ACS values for pre-force-fed "healthy" livers are in accordance with tabulated data for mammal livers (Duck 1990). The liver fat fraction at day 7 of force-feeding has been reported to range between 30% to 40% (Baéza et al. 2013). The ACS mean value of 0.91 dB/cm/MHz found at day 7 may therefore correspond to attenuation estimation reported in steatosis grade 3 human patients (Sasso et al. 2010; Karlas et al. 2017). However, based on current literature on human fatty livers (Sasso et al. 2010, 2012, 2016; Karlas et al. 2017; Tada et al. 2019b), it was genuinely expected that ACS would continue to increase at higher fat fractions. On the contrary, a decrease in local ACS was observed on day 14, and this is likely explained by the very high fat fraction of fed ducks (steatosis grade 3 with >95% of hepatocytes containing fat; Fig. 3).

To validate the latter hypothesis and eliminate the possibility of artifactual measures on day 14, supplementary experiments were conducted on custom-made local attenuation tissue-mimicking phantoms with ACS values of 1.6 and 0.85 dB/cm/MHz (see Appendix). The point here was to prove that ACS could properly be estimated even in situations of jeopardized SNR because of abdominal fat, as encountered during fed duck experiments. Those phantoms were imaged with the same settings, with or without an intervening layer of duck fat. Local ACS values were obtained using the SLD method. With both configurations, as summarized in the Appendix, ACS values in accordance with reference methods were found. This allowed demonstration of the ability of the SLD method to measure high values of local ACS (*i.e.*, values similar or higher than those reported in Fig. 2), in agreement with other SLD-based studies (McFarlin et al. 2010; Coila and Lavarello 2018). This observation thus indicates that if such high values of ACS (*i.e.*, >0.91 dB/cm/MHz as in day 7) had occurred in duck experiments, it would have been possible to reliably estimate them, and henceforth this supports the validity of data obtained at day 14.

Accordingly, the reduction of local ACS values between days 7 and 14 should lie in the cellular structure of the liver at such extreme fat fractions. Davies et al. (1991) reported a similar surprising lack of attenuation in three human clinical cases showing "the grossest possible fatty change." Even though rarity of such human cases and the qualitative nature of the examination performed at that time make comparison delicate, their hypothesis to explain this lack of attenuation may apply to *foie gras* as well.

In the following lines, we aim to further explain the reduction of ACS on day 14 and the potential impact of scattering on attenuation. Ultrasound attenuation in tissues is a combination of absorption and scattering. Local ACS can be modeled as $\alpha_{att} = \alpha_{abs} + \alpha_{scatt}$, where α_{abs} and α_{scatt} are absorption and scattering coefficients, respectively. The absorption coefficient of healthy human livers is about 0.4 dB/cm/MHz (Duck 1990). This, combined with low scattering, causes absorption to be the main cause of attenuation in healthy and fatless livers (Lyons and Parker 1988). The fat absorption tabulated in mammals is similar to that of humans at about 0.4 dB/cm/MHz (Goldman and Hueter 1956; Goss et al. 1978). As the fat chemical composition is grossly the same for mammals, ducks and geese (Hilditch 1949; Laurell and Lundquist 1971; Valeri and Meirelles 1997; Kotronen et al. 2010; Carrillo et al. 2017), ultrasound absorption in duck fat is thus expected to be also around 0.4 dB/cm/MHz.

For a homogeneous mix of liver hepatocytes and fat, α_{abs} is a mass fraction-weighted average of fat and liver absorption. Therefore, α_{abs} should remain within the range 0.4−0.5 dB/cm/MHz, whatever the fat fraction. This argument supports the conclusion of Narayana and Ophir (1983) and Taylor et al. (1986), stipulating that attenuation variations between healthy and fatty livers are dominated by scattering caused by microscopic fat vacuoles in hepatic cells. As long as steatosis remains mild, fat infiltrates the liver under the form of microvacuoles, acting as new inserted acoustic scatterers. But past a certain point, fat infiltration leads several microvacuoles to coalesce into single bigger macrovacuoles, as seen in the duck 15 liver specimen (see Fig. 3), which now act as weaker scatterers that fill more than half of hepatocytes (Locsmándi et al. 2007). This change in liver structure at a high fat fraction could explain the decrease in attenuation on day 14, as 95% of hepatocytes contained coalesced macrovacuoles of fat (in the shown duck 15 liver specimen).

*Homodyned-*K *feature estimation*

This hypothesis of a change in the scattering regime is also suggested by HKD feature trends. The inverse relationship between the mean scattering intensity μ_n and local attenuation ACS could be expected, as ACS is dominated by scattering. The reciprocal $1/\alpha$ of the

scatterer clustering parameter can be interpreted as a marker of either heterogeneity or the effective density of random scatterers, whereas the coherent-to-diffuse signal ratio k is an indicator of structure in scatterer spatial organization, from fully random to crystalline structure (Dutt and Greenleaf 1994; Destrempes and Cloutier 2010).

Before day 7, results indicate an increase in scatterer density and homogeneity of fluctuations in acoustical impedance, on one hand, and a decrease in scatterer structural organization, on the other hand. This supports the hypothesis that microvacuoles are randomly spaced. After day 7, the coalescence of vacuoles and ballooning of hepatocytes gave the medium a more crystalline organization in duck 15 (Fig. 3). Although self-consistent and in accordance with previous works, additional validations would be needed to help understand why the observed non-monotonicity in HKD feature $1/\alpha$ did not match its expected strictly decreasing behavior reported in previous studies (Ghoshal et al. 2012; Fang et al. 2018).

To add on this latter observation, it must be said that there are differences in methodology for HKD feature estimation between our team's work and other publications. Namely, when computing HKD parametric maps in Fang et al. (2018) and Ghoshal et al. (2012), it was assumed that the echo envelope within a given sliding window could be modeled by a single homodyned K-distribution. But as this might not necessarily be the case, the method used in this study allowed for the presence of multiple homodyned K-distributions, as in Destrempes et al. (2016), through the use of pixel classification within estimation windows with three or fewer (statistical echogenicity) labels. To assess to which extent multiple distributions did occur in the context of this study (*i.e.*, a number of labels greater than 1), Shannon's entropy $H(\vec{p}) = -\sum_{i=1}^{3} p_i \log p_i$ on proportions $\vec{p} = (p_1, p_2, p_3)$ of distribution labels within sliding windows was computed. Mean values ± SD at the four time points were 0.55 ± 0.13 (day −12), 0.54 ± 0.13 (day 0), 0.33 ± 0.07 (day 7) and 0.46 ± 0.08 (day 14). As Shannon entropy would be zero if there were only single homodyned K-distributions within each window, these results indicate that the more general hypothesis of multiple distributions that we have adopted is unavoidable.

Ultrasound acquisitions

QUS estimation is usually applied to conventionally focused beamforming. In this study, our choice to use plane wave imaging was motivated by the fact that because of an unavoidable motion of ducks, it was preferable to benefit from the rapidity of acquisitions provided by plane wave beamforming, despite its lower SNR. Nevertheless, it should be noted that QUS with plane wave imaging has been proven feasible (Lavarello 2013; Garcia-Duitama et al. 2015) and that leveraging angular compounding can increase the frame rate, while preserving signal quality and stabilizing spatial variability across parametric maps (Salles et al. 2014).

The shear wave tracking frame rate (of 3623 Hz) is dictated by the temporal sampling of the shear wave propagation, and it was selected within common ranges reported in shear wave elasticity and viscoelasticity human liver studies (for instance, 5000 Hz in Budelli et al. [2017], 4800 Hz in Nightingale et al. [2015] or 2770 Hz in Amador et al. [2016]). To prevent strong motion artifacts in non-anesthetized moving ducks with non-momentarily interrupted breathing, we used only three compounding angles in this study. We plan to use the motion compensation method of Porée et al. (2016) in future works, thus allowing for more compounding angles.

Future works

In the study described here, various features arising from mechanical and acoustical properties of biological tissues were studied individually, but note that in the context of detection or classification based on machine learning, one would consider combinations of these features for better performance, as was reported previously in a rat model of steatohepatitis (Tang et al. 2019). In the framework of multiparametric imaging and machine learning, other features could also be investigated to increase classification performance. By use of the same data set, the backscatter coefficient estimated with a spectral fit algorithm would complement our hypothesis on a change in scattering regime for *foie gras*. Even though it has been reported that the spectral based backscatter coefficient can be linked to one of the HKD features (Destrempes et al. 2016), adding some redundancy can be profitable in machine learning context (Guyon and Elisseeff 2003). Note, however, that our cohort consisted of only 16 ducks, which constitute rather a small data set for including any machine learning-based analysis in the present study. However, raising ducks in the farmhouse is a seasonal process, and we hope to increase the size of our database over the year, which could pave the way for such a study in the future.

For future studies, the versatility of Verasonics programmable scanners could also be leveraged to allow for the implementation of other ultrasound emission modes. For instance, the tissue Green's function estimation proposed by Imbault et al. (2017) to estimate the speed of sound in livers has been proven to be a promising estimator of fat fraction (Kumagai et al. 2014; Imbault et al. 2018; Dioguardi Burgio et al. 2019). This could be a feature to consider.

Corresponding histology for each duck liver sample could not be obtained in the present study. The ducks were being raised in a farmhouse for commercial production of *foie gras*. Thus, sacrificing more than one duck was out of scope; animal manipulations were supervised by a veterinarian, and any histology sample handling discarded the animal from food commercialization. Consequently, the lack of histology over the entire database restricted the interpretation of our results. Even though the fat fraction was not available at each time point during force-feeding, there was nevertheless a visual assessment by the *foie gras* producers after slaughtering to confirm that livers were fatty and considered as *foie gras*. Note that fattening of ducks' livers along force-feeding was reported in Bonnefont et al. (2019). In the latter study, the liver lipid content was shown to progressively increase from day 0 to day 12 (no data available at day 14). Future protocols not performed in the context of food production may allow providing histology at each time point to support interpretation of results. This may also allow elucidation of observed modal relations between QUS parameters and histology-confirmed fat liver content. This would also allow supporting QUS observations made recently in patients with liver steatosis (Han et al. 2019). Indeed, in the latter report, non-linear modal relations between QUS parameters and the fat fraction determined by magnetic resonance imaging were observed. This finding from a clinical data set seems to agree with modal relations of QUS parameters versus force-feeding time points reported here.

Finally, the method described here is easily adaptable to human clinical trials on NASH by use of a lower-frequency curved array probe. However, it is expected that some of the trends observed in this study might be different, such as stiffness in steatosis (Deffieux et al. 2015; Nightingale et al. 2015), because of evident differences between a fat intake induced in 2 wk in ducks and a disease that can take years to develop in humans.

CONCLUSIONS

We developed a multiparametric ultrasound imaging workflow for steatosis monitoring in duck livers during force-feeding. Six ultrasound biomarkers were investigated. Using shear wave elastography, we found that duck *foie gras* becomes stiffer and more dispersive, but those measurements become unreliable toward the end of the fattening process. To overcome this difficulty, significant trends in local ACS and HKD features along the feeding process could be leveraged, keeping in mind that these trends are not monotonic, possibly because of a change in ultrasound scattering regime at high liver fat fractions. Nevertheless, combining these six features might allow for better classification. Finally, this study has proposed a pre-clinical model that might be advantageous for fundamental research in QUS as the proposed model allowed the development of different grades of steatosis without fibrosis.

Acknowledgments—This work was supported by AUDACE Grant 2019-AUDC-263591 from the Fonds de Recherche du Québec. A.T. was supported by a research scholarship from the Fonds de Recherche du Québec en Santé and Fondation de l'Association des Radiologistes du Québec Junior 2 Salary Award (FRQS-ARQ 34939). We also thank Fernande Ouellet and Francis Laroche, *foie gras* producers (Rusé comme un canard farm, Granby, QC, Canada); veterinarian Nathalie Vermette, who performed ultrasound examinations; and Boris Chayer for his technical support and advice.

Conflict of interest disclosure—The authors have no conflicts of interest to disclose.

APPENDIX

Validation of the ACS estimation

The SLD algorithm being a local ACS estimator, it should not depend strongly on subcutaneous fat and aberration between the ultrasound probe and parameter estimation regions. Furthermore, it has been shown to reliably estimate ACS values as high as 1.6 dB/cm/MHz (Coila and Lavarello 2018; McFarlin et al. 2010). However, for further validation, phantom experiments were performed.

Two batches (#1 and #2) of attenuating tissue mimicking phantoms were prepared, mixing recipes from Madsen et al. (1978) and Rickey et al. (1995). We used 2% of agar (A9799, Sigma Aldrich) in water before heating. Once the agar was dissolved in boiling water, graphite powder (282863, Sigma Aldrich) was added − 19% for batch #1 and 13% for batch #2. Once graphite was incorporated, 8% glycerol was introduced to the hot mix. Phantoms were cast side by side in a mold surrounded by ice. Glycerol was viscous enough to prevent sedimentation of graphite particles and it also allowed to increase the speed of sound to a value closer to that of biological tissues. Once the phantom was set, a 2 cm long piece was calibrated using a transmission/reflection technique with a planar Plexiglas reflector in a degased water tank (Madsen et al. 1999; Wear et al. 2005). Speeds of sound in phantoms were measured at 1530 ± 1 m/s and 1533 ± 1 m/s, and ACS values were 1.60 ± 0.03 dB/cm/MHz and 0.85 ± 0.03 dB/cm/MHz for batches #1 and #2, respectively. Phantoms were imaged at room temperature following the same imaging protocol as used for ducks, with and without a layer of rendered duck fat (Brome Lake Ducks LTD, Knowlton, Quebec, Canada) of approximately 1 cm thick between the probe and the phantom. ACS was estimated using the SLD method and averaged over the homogeneous part of the phantom. Similarly to ducks, acquisitions were repeated 4 times using different imaging views of the phantom.

Table 2. Attenuation coefficient slope values in the two batches of tissue-mimicking phantoms*

Batch	Attenuation coefficient slope (dB/cm/MHz)					
	Ground truth		SLD without duck fat		SLD with duck fat	
	Mean	SD	Mean	SD	Mean	SD
1	1.60	0.03	1.64	0.06	1.43	0.18
2	0.85	0.03	0.88	0.09	1.07	0.15

SD = standard deviation; SLD = spectral log difference.
*Ground truth values are compared with SLD estimated values with and without a 1-cm duck fat layer between the probe and the phantom. The "mean" represents the averaged value over the four acquisitions.

Table 2 is reporting averaged values over 4 acquisitions as well as corresponding standard deviations. Without the fat layer, SLD yielded consistent ACS values with respect to ground truths. ACS obtained with a layer of fat showed a greater variability and a bias probably due to ultrasound phase aberrations. However, obtained values stayed consistent within the uncertainty range and both batches could be discriminated. Hence, those results are suggesting that ACS values on duck livers at d14 were not artifacts.

REFERENCES

Amador C, Song P, Meixner DD, Chen S, Urban MW. Improvement of shear wave motion detection using harmonic imaging in healthy human liver. Ultrasound Med Biol 2016;42:1031–1041.

Baéza E, Marie-Etancelin C, Davail S, Diot C. La stéatose hépatique chez les palmipèdes. INRA Prod Anim 2013;26:403–414.

Barry CT, Mills B, Hah Z, Mooney RA, Ryan CK, Rubens DJ, Parker KJ. Shear wave dispersion measures liver steatosis. Ultrasound Med Biol 2012;38:175–182.

Barry CT, Hah Z, Partin A, Mooney RA, Chuang KH, Augustine A, Almudevar A, Cao W, Rubens DJ, Parker KJ. Mouse liver dispersion for the diagnosis of early-stage fatty liver disease: A 70-sample study. Ultrasound Med Biol 2014;40:704–713.

Barry CT, Hazard C, Hah Z, Cheng G, Partin A, Mooney RA, Chuang KH, Cao W, Rubens DJ, Parker KJ. Shear wave dispersion in lean versus steatotic rat livers. J Ultrasound Med 2015;34:1123–1129.

Bernard S, Kazemirad S, Cloutier G. A frequency-shift method to measure shear-wave attenuation in soft tissues. IEEE Trans Ultrason Ferroelectr Freq Control 2017;64:514–524.

Bhatt M, Moussu MAC, Chayer B, Destrempes F, Gesnik M, Allard L, Tang A, Cloutier G. Reconstruction of viscosity maps in ultrasound shear wave elastography. IEEE Trans Ultrason Ferroelectr Freq Control 2019;66:1065–1078.

Bonekamp S, Tang A, Mashhood A, Wolfson T, Changchien C, Middleton MS, Clark L, Gamst A, Loomba R, Sirlin CB. Spatial distribution of MRI-determined hepatic proton density fat fraction in adults with nonalcoholic fatty liver disease. J Magn Reson Imaging 2014;39:1525–1532.

Bonnefont CM, Molette C, Lavigne F, Manse H, Bravo C, Lo B, Rémignon H, Arroyo J, Bouillier-Oudot M. Evolution of liver fattening and foie gras technological yield during the overfeeding period in mule duck. Poultry Science 2019;98:5724–5733.

Bouchard RR, Hsu SJ, Wolf PD, Trahey GE. In vivo cardiac, acoustic-radiation-force-driven, shear wave velocimetry. Ultrason Imaging 2009;31:201–213.

Budelli E, Brum J, Bernal M, Deffieux T, Tanter M, Lema P, Negreira C, Gennisson JL. A diffraction correction for storage and loss moduli imaging using radiation force based elastography. Phys Med Biol 2017;62:91–106.

Carrillo FS, Saucier L, Ratti C. Thermal properties of duck fatty liver (foie gras) products. Int J Food Prop 2017;20:573–584.

Castera L, Friedrich-Rust M, Loomba R. Noninvasive assessment of liver disease in patients with nonalcoholic fatty liver disease. Gastroenterology 2019;156 1264−1281.e4.

Chen S, Fatemi M, Greenleaf JF. Quantifying elasticity and viscosity from measurement of shear wave speed dispersion. J Acoust Soc Am 2004;115:2781–2785.

Coila AL, Lavarello RJ. Regularized spectral log difference technique for ultrasonic attenuation imaging. IEEE Trans Ultrason Ferroelectr Freq Control 2018;65:378–389.

Correia M, Provost J, Chatelin S, Villemain O, Tanter M, Pernot M. Ultrafast harmonic coherent compound (UHCC) imaging for high frame rate echocardiography and shear-wave elastography. IEEE Trans Ultrason Ferroelectr Freq Control 2016;63:420–431.

Davies RJ, Saverymuttu SH, Fallowfield M, Joseph AEA. Paradoxical lack of ultrasound attenuation with gross fatty change in the liver. Clin Radiol 1991;43:393–396.

De Lédinghen V, Vergniol J, Capdepont M, Chermak F, Hiriart JB, Cassinotto C, Merrouche W, Foucher J, Brigitte LB. Controlled attenuation parameter (CAP) for the diagnosis of steatosis: A prospective study of 5323 examinations. J Hepatol 2014;60:1026–1031.

Deffieux T, Montaldo G, Tanter M, Fink M. Shear wave spectroscopy for in vivo quantification of human soft tissues visco-elasticity. IEEE Trans Med Imaging 2009;28:313–322.

Deffieux T, Gennisson JL, Bousquet L, Corouge M, Cosconea S, Amroun D, Tripon S, Terris B, Mallet V, Sogni P, Tanter M, Pol S. Investigating liver stiffness and viscosity for fibrosis, steatosis and activity staging using shear wave elastography. J Hepatol 2015;62:317–324.

Destrempes F, Cloutier G. A critical review and uniformized representation of statistical distributions modeling the ultrasound echo envelope. Ultrasound Med Biol 2010;36:1037–1051.

Destrempes F, Cloutier G. Review of envelope statistics models for quantitative ultrasound imaging and tissue characterization. In: Mamou J, Oelze ML, (eds). Quantitative ultrasound in soft tissues. Dordrecht: Springer; 2013. p. 219–274.

Destrempes F, Franceschini E, Yu FTH, Cloutier G. Unifying concepts of statistical and spectral quantitative ultrasound techniques. IEEE Trans Med Imaging 2016;35:488–500.

Dioguardi Burgio M, Imbault M, Ronot M, Faccinetto A, Van Beers B, Rautou PE, Castera L, Gennisson JL, Tanter M, Vilgrain V. Ultrasonic adaptive sound speed estimation for the diagnosis and quantification of hepatic steatosis: A pilot study. Ultraschall Med 2019;40:722–733.

Duck FA. Physical properties of tissue: A comprehensive reference book. London: Academic Press; 1990.

Dutt V, Greenleaf JF. Ultrasound echo envelope analysis using a homodyned *K* distribution signal model. Ultrason. Imaging 1994;16:265–287.

Fang J, Zhou Z, Chang NF, Wan YL, Tsui PH. Ultrasound parametric imaging of hepatic steatosis using the homodyned-*K* distribution: An animal study. Ultrasonics 2018;87:91–102.

Franceschini E, Escoffre JM, Novell A, Auboire L, Mendes V, Benane YM, Bouakaz A, Basset O. Quantitative ultrasound in ex vivo fibrotic rabbit livers. Ultrasound Med Biol 2019;45:1777–1786.

Gallot T, Catheline S, Roux P, Brum J, Benech N, Negreira C. Passive elastography: Shear-wave tomography from physiological-noise correlation in soft tissues. IEEE Trans Ultrason Ferroelectr Freq Control 2011;58:1122–1126.

Garcia D, Le Tarnec L, Muth S, Montagnon E, Porée J, Cloutier G. Stolt's f-k migration for plane wave ultrasound imaging. IEEE Trans Ultrason Ferroelectr Freq Control 2013;60:1853–1867.

Garcia-Duitama J, Chayer B, Han A, Garcia D, Oelze ML, Cloutier G. Experimental application of ultrafast imaging to spectral tissue characterization. Ultrasound Med Biol 2015;41:2506–2519.

Ghoshal G, Lavarello RJ, Kemmerer JP, Miller RJ, Oelze ML. Ex vivo study of quantitative ultrasound parameters in fatty rabbit livers. Ultrasound Med Biol 2012;38:2238–2248.

Goldman DE, Hueter TF. Tabular data of the velocity and absorption of high−frequency sound in mammalian tissues. J Acoust Soc Am 1956;28:35–37.

Goss SA, Johnston RL, Dunn F. Comprehensive compilation of empirical ultrasonic properties of mammalian tissues. J Acoust Soc Am 1978;64:423–457.
Guyon I, Elisseeff A. An introduction to variable and feature selection. J Mach Learn Res 2003;3:1157–1182.
Han A, Boehringer AS, Zhang YN, Montes V, Andre MP, Erdman JW, Loomba R, Sirlin CB, O'Brien WD. Improved assessment of hepatic steatosis in humans using multi-parametric quantitative ultrasound. Proc IEEE Int Ultrason Symp 2019;1819–1822.
Hermier D, Salichon MR, Guy G, Peresson R, Mourot J, Lagarrigue S. La stéatose hépatique des palmipèdes gavés: Bases métaboliques et sensibilité génétique. Prod Anim 1999;12:265–271.
Hilditch TP. The chemical constitution of natural fats. Br J Nutr 1949;3:347–354.
Imbault M, Faccinetto A, Osmanski BF, Tissier A, Deffieux T, Gennisson JL, Vilgrain V, Tanter M. Robust sound speed estimation for ultrasound-based hepatic steatosis assessment. Phys Med Biol 2017;62:3582–3598.
Imbault M, Burgio MD, Faccinetto A, Ronot M, Bendjador H, Deffieux T, Triquet EO, Rautou PE, Castera L, Gennisson JL, Vilgrain V, Tanter M. Ultrasonic fat fraction quantification using in vivo adaptive sound speed estimation. Phys Med Biol 2018;63 215013.
Insana M, Zagzebski J, Madsen EL. Improvements in the spectral difference method for measuring ultrasonics attenuation. Ultrason Imaging 1983;5:331–345.
Karlas T, Petroff D, Sasso M, Fan JG, Mi YQ, de Lédinghen V, Kumar M, Lupsor-Platon M, Han KH, Cardoso AC, Ferraioli G, Chan WK, Wong VWS, Myers RP, Chayama K, Friedrich-Rust M, Beaugrand M, Shen F, Hiriart JB, Sarin SK, Badea R, Jung KS, Marcellin P, Filice C, Mahadeva S, Wong GLH, Crotty P, Masaki K, Bojunga J, Bedossa P, Keim V, Wiegand J. Individual patient data meta-analysis of controlled attenuation parameter (CAP) technology for assessing steatosis. J Hepatol 2017;66:1022–1030.
Kazemirad S, Zhang E, Nguyen BN, Bodson-Clermont P, Destrempes F, Trudel D, Cloutier G, Tang A. Detection of steatohepatitis in a rat model by using spectroscopic shear-wave US elastography. Radiology 2017;282:726–733.
Kleiner DE, Brunt EM, Van Natta M, Behling C, Contos MJ, Cummings OW, Ferrell LD, Liu YC, Torbenson MS, Unalp-Arida A, Yeh M, McCullough AJ, Sanyal AJ. Design and validation of a histological scoring system for nonalcoholic fatty liver disease. Hepatology 2005;41:1313–1321.
Kotronen A, Seppänen-laakso T, Westerbacka J, Kiviluoto T, Arola J, Ruskeepää A, Yki-järvinen H, Orešič M. Comparison of lipid and fatty acid composition of the liver, subcutaneous and intra-abdominal adipose tissue, and serum. Obesity 2010;18:937–944.
Kumagai H, Yokoyama K, Katsuyama K, Hara S, Yamamoto H, Yamagata T, Taniguchi N, Hirota N, Itoh K. A new method for measuring the speed of sound in rat liver ex vivo using an ultrasound system: Correlation of sound speed with fat deposition. Ultrasound Med Biol 2014;40:2499–2507.
Labyed Y, Bigelow TA. A theoretical comparison of attenuation measurement techniques from backscattered ultrasound echoes. J Acoust Soc Am 2011;129:2316–2324.
Laurell S, Lundquist A. Lipid composition of human liver biopsy specimens. Acta Med Scand 1971;189:65–68.
Lavarello RJ. Estimation of quantitative ultrasound parameters derived from backscatter coefficients using plane wave compounding: A comparative simulation study. IEEE Int Ultrason Symp 2013;421–424.
Lee DH, Lee JY, Lee KB, Han JK. Evaluation of hepatic steatosis by using acoustic structure quantification US in a rat model: Comparison with pathologic examination and MR spectroscopy. Radiology 2017;285:445–453.
Lin SC, Heba E, Wolfson T, Ang B, Gamst A, Han A, Erdman JW, O'Brien WD, Andre MP, Sirlin CB, Loomba R. Noninvasive diagnosis of nonalcoholic fatty liver disease and quantification of liver fat using a new quantitative ultrasound technique. Clin Gastroenterol Hepatol 2015;13:1337–1345.
Lin YH, Liao YY, Yeh CK, Yang KC, Tsui PH. Ultrasound entropy imaging of nonalcoholic fatty liver disease: Association with metabolic syndrome. Entropy 2018;20:1–16.
Locsmándi L, Hegedüs G, Andrássy-Baka G, Bogenfürst F, Romvári R. Following the goose liver development by means of cross-sectional digital imaging, liver histology and blood biochemical parameters. Acta Biol Hung 2007;58:35–48.
Loomba R. Role of imaging-based biomarkers in NAFLD: Recent advances in clinical application and future research directions. J Hepatol 2018;68:296–304.
Loupas T, Powers JT, Gill RW. An axial velocity estimator for ultrasound blood flow imaging, based on a full evaluation of the Doppler equation by means of a two-dimensional autocorrelation approach. IEEE Trans Ultrason Ferroelectr Freq Control 1995;42:672–688.
Lyons ME, Parker KJ. Absorption and attenuation in soft tissues: II. Experimental results. IEEE Trans Ultrason Ferroelectr Freq Control 1988;35:511–521.
Madsen EL, Zagzebski JA, Banjavie RA, Jutila RE. Tissue mimicking materials for ultrasound phantoms. Med Phys 1978;5:391–394.
Madsen EL, Dong F, Frank GR, Garra BS, Wear KA, Wilson T, Zagzebski JA, Miller HL, Shung KK, Wang SH, Feleppa EJ, Liu T, Brien WDO, Topp KA, Sanghvi NT, Zaitsev AV, Hall TJ, Fowlkes JB, Kripfgans OD, Miller JG. Interlaboratory comparison of ultrasonic backscatter, attenuation, and speed measurements. J Ultrasound Med 1999;18:615–631.
McFarlin BL, Bigelow TA, Laybed Y, O'Brien WDJ, Oelze ML, Abramowicz JS. Ultrasonic attenuation estimation of the pregnant cervix : a preliminary report. Ultrasound Obstet Gynecol 2010;36:218–228.
Moore CJ, Caughey MC, Meyer DO, Emmett R, Jacobs C, Chopra M, Howard JF, Jr, Gallippi CM. In vivo viscoelastic response (VisR) ultrasound for characterizing mechanical anisotropy in lower-limb skeletal muscles of boys with and without Duchenne muscular dystrophy. Ultrasound Med Biol 2018;44:2519–2530.
Nam K, Zagzebski JA, Hall TJ. Simultaneous backscatter and attenuation estimation using a least squares method with constraints. Ultrasound Med Biol 2011;37:2096–2104.
Narayana PA, Ophir J. On the frequency dependence of attenuation in normal and fatty liver IEEE. Trans Sonics Ultrason 1983;30:379–382.
Nightingale K, Rouze N, Rosenzweig S, Wang M, Abdelmalek M, Guy C, Palmeri M. Derivation and analysis of viscoelastic properties in human liver: Impact of frequency on fibrosis and steatosis staging IEEE. Trans Ultrason Ferroelectr Freq Control 2015;62:165–175.
Ozturk A, Grajo JR, Gee MS, Benjamin A, Zubajlo R, Thomenius K, Anthony B, Samir A, Dhyani M. Quantitative hepatic fat quantification in non-alcoholic fatty liver disease using ultrasound-based techniques: A review of literature and their diagnostic performance. Ultrasound Med Biol Biol 2018;44:2461–2475.
Parker KJ, Ormachea J, Will S, Hah Z. Analysis of transient shear wave in lossy media. Ultrasound Med Biol 2018;44:1504–1515.
Porée J, Posada D, Hodzic A, Tournoux F, Cloutier G, Garcia D. High-frame-rate echocardiography using coherent compounding with Doppler-based motion-compensation. IEEE Trans Med Imaging 2016;35:1647–1657.
Qu Y, Li M, Hamilton G, Zhang YN, Song B. Diagnostic accuracy of hepatic proton density fat fraction measured by magnetic resonance imaging for the evaluation of liver steatosis with histology as reference standard: a meta-analysis. Eur Radiol 2019;29:5180–5189.
Ricci C, Longo R, Gioulis E, Bosco M, Pollesello P, Masutti F, Crocè LS, Paoletti S, Bernard B, De Tiribelli C, Palma LD. Noninvasive in vivo quantitative assessment of fat content in human liver. J Hepatol 1997;27:108–113.
Rickey DW, Picot PA, Christopher DA, Fenster A. A wall-less vessel phantom for Doppler ultrasound studies. Ultrasound Med Biol 1995;21:1163–1176.
Rouze NC, Deng Y, Trutna CA, Palmeri ML, Nightingale KR. Characterization of viscoelastic materials using group shear wave speeds. IEEE Trans Ultrason Ferroelectr Freq Control 2018;65:780–794.
Salles S, Liebgott H, Basset O, Cachard C, Vray D, Lavarello R. Experimental evaluation of spectral-based quantitative ultrasound imaging using plane wave compounding. IEEE Trans Ultrason Ferroelectr Freq Control 2014;61:1824–1834.

Sanyal AJ, Brunt EM, Kleiner DE, Kowdley KV, Chalasani N, Lavine JE, Ratziu V, Mccullough A. Endpoints and clinical trial design for nonalcoholic steatohepatitis. Hepatology 2011;54:344–353.

Sasso M, Beaugrand M, de Ledinghen V, Douvin C, Marcellin P, Poupon R, Sandrin L, Miette V. Controlled attenuation parameter (CAP): A novel VCTE™ guided ultrasonic attenuation measurement for the evaluation of hepatic steatosis: Preliminary study and validation in a cohort of patients with chronic liver disease from various causes. Ultrasound Med Biol 2010;36:1825–1835.

Sasso M, Miette V, Sandrin L, Beaugrand M. The controlled attenuation parameter (CAP): A novel tool for the non-invasive evaluation of steatosis using Fibroscan®. Clin Res Hepatol Gastroenterol 2012;36:13–20.

Sasso M, Audière S, Kemgang A, Gaouar F, Corpechot C, Chazouillères O, Fournier C, Golsztejn O, Prince S, Menu Y, Sandrin L, Miette V. Liver steatosis assessed by controlled attenuation parameter (CAP) measured with the XL probe of the FibroScan: A pilot study assessing diagnostic accuracy. Ultrasound Med Biol 2016;42:92–103.

Sharma AK, Reis J, Oppenheimer DC, Rubens DJ, Ormachea J, Hah Z, Parker KJ. Attenuation of shear waves in normal and steatotic livers. Ultrasound Med Biol 2019;45:895–901.

Szabo TL. Diagnostic ultrasound imaging: inside out. London: Academic Press; 2004.

Tabaru M, Azuma T, Hashiba K. Measurement of elastic properties of tissue by shear wave propagation generated by acoustic radiation force. Jpn J Appl Phys 2010;49:07HF09.

Tada T, Kumada T, Toyoda H, Kobayashi N, Sone Y, Oguri T, Kamiyama N. Utility of attenuation coefficient measurement using an ultrasound-guided attenuation parameter for evaluation of hepatic steatosis: Comparison with MRI-determined proton density fat fraction. Am J Roentgenol 2019a;212:332–341.

Tada T, Iijima H, Kobayashi N, Yoshida M, Nishimura T, Kumada T, Kondo R, Yano H, Kage M, Nakano C, Aoki T, Aizawa N, Ikeda N, Takashima T, Yuri Y, Ishii N, Hasegawa K, Takata R, Yoh K, Sakai Y, Nishikawa H, Iwata Y, Enomoto H, Hirota S, Fujimoto J, Nishiguchi S. Usefulness of attenuation imaging with an ultrasound scanner for the evaluation of hepatic steatosis. Ultrasound Med Biol 2019b;45:2679–2687.

Tang A, Destrempes F, Kazemirad S, Garcia-Duitama J, Nguyen BN, Cloutier G. Quantitative ultrasound and machine learning for assessment of steatohepatitis in a rat model. Eur Radiol 2019;29:2175–2184.

Taylor KJW, Riely CA, Hammers L, Flax S, Weltin G, Tsao-Garcia G, Conn HO, Kuc R, Barwick KW. Quantitative US attenuation in normal liver and in patients with diffuse liver disease: importance of fat. Radiology 1986;160:65–71.

Vajihi Z, Rosado-Mendez IM, Hall TJ, Rivaz H. Low variance estimation of backscatter quantitative ultrasound parameters using dynamic programming. IEEE Trans Ultrason Ferroelectr Freq Control 2018;65:2042–2053.

Valeri D, Meirelles AJA. Viscosities of fatty acids, triglycerides, and their binary mixtures. J Am Oil Chem Soc 1997;74:1221–1226.

Vernon G, Baranova A, Younossi ZM. Systematic review: the epidemiology and natural history of non-alcoholic fatty liver disease and non-alcoholic steatohepatitis in adults. Aliment Pharmacol Ther 2011;34:274–285.

Wear KA, Stiles TA, Frank GR, Madsen EL, Cheng F, Feleppa EJ, Hall CS, Soo B, Lee P, O'Brien WDO, Oelze ML, Raju BI, Shung KK, Wilson T, Yuan JR. Interlaboratory comparison of ultrasonic backscatter coefficient measurements from 2 to 9 MHz. J Ultrasound Med 2005;24:1235–1250.

Weltman MD, Farrell GC, Liddle C. Increased hepatocyte CYP2 E1 expression in a rat nutritional model of hepatic steatosis with inflammation. Gastroenterology 1996;111:1645–1653.

Yokoo T, Serai SD, Pirasteh A, Bashir MR, Hamilton G, Hernando D, Hu HH, Hetterich H, Kühn JP, Kukuk GM, Loomba R, Middleton MS, Obuchowski NA, Song JS, Tang A, Wu X, Reeder SB, Sirlin CB. Linearity, bias, and precision of hepatic proton density fat fraction measurements by using MR imaging: A meta-analysis. Radiology 2018;286:486–498.

Yu FTH, Franceschini É, Chayer B, Armstrong JK, Meiselman HJ, Cloutier G. Ultrasonic parametric imaging of erythrocyte aggregation using the structure factor size estimator. Biorheology 2009;46:343–363.

Zhang YN, Fowler KJ, Hamilton G, Cui JY, Sy EZ, Balanay M, Hooker JC, Szeverenyi N, Sirlin CB. Liver fat imaging—A clinical overview of ultrasound, CT, and MR imaging. Br J Radiol 2018;91 20170959.

Zhou Z, Zhang Q, Wu W, Wu S, Tsui PH. Hepatic steatosis assessment using quantitative ultrasound parametric imaging based on backscatter envelope statistics. Appl Sci 2019;9:661.